Deep ocean warming assessed from altimeters, Gravity Recovery and Climate Experiment, in situ measurements, and a non-Boussinesq ocean general circulation model

Y. Tony Song[1] and Frank Colberg[1,2]

Received 16 August 2010; revised 15 October 2010; accepted 7 December 2010; published 15 February 2011.

[1] Observational surveys have shown significant oceanic bottom water warming, but they are too spatially and temporally sporadic to quantify the deep ocean contribution to the present-day sea level rise (SLR). In this study, altimetry sea surface height (SSH), Gravity Recovery and Climate Experiment (GRACE) ocean mass, and in situ upper ocean (0–700 m) steric height have been assessed for their seasonal variability and trend maps. It is shown that neither the global mean nor the regional trends of altimetry SLR can be explained by the upper ocean steric height plus the GRACE ocean mass. A non-Boussinesq ocean general circulation model (OGCM), allowing the sea level to rise as a direct response to the heat added into the ocean, is then used to diagnose the deep ocean steric height. Constrained by sea surface temperature data and the top of atmosphere (TOA) radiation measurements, the model reproduces the observed upper ocean heat content well. Combining the modeled deep ocean steric height with observational upper ocean data gives the full depth steric height. Adding a GRACE-estimated mass trend, the data-model combination explains not only the altimetry global mean SLR but also its regional trends fairly well. The deep ocean warming is mostly prevalent in the Atlantic and Indian oceans, and along the Antarctic Circumpolar Current, suggesting a strong relation to the oceanic circulation and dynamics. Its comparison with available bottom water measurements shows reasonably good agreement, indicating that deep ocean warming below 700 m might have contributed 1.1 mm/yr to the global mean SLR or one-third of the altimeter-observed rate of 3.11 ± 0.6 mm/yr over 1993–2008.

Citation: Song, Y. T., and F. Colberg (2011), Deep ocean warming assessed from altimeters, Gravity Recovery and Climate Experiment, in situ measurements, and a non-Boussinesq ocean general circulation model, *J. Geophys. Res.*, *116*, C02020, doi:10.1029/2010JC006601.

1. Introduction

[2] Assessing present-day sea level changes has been an important component of the 2007 Intergovernmental Panel for Climate Change (IPCC) report, and it can have societal implications because of the possibility of sea level rise (SLR) acceleration and consequent threat to many low lying parts of the inhabited world [*Church et al.*, 2010]. Satellite altimeters have observed a global mean SLR of 3.11 ± 0.6 mm/yr since 1993–2008 [*Ablain et al.*, 2009]. In theory, the SLR should be explained by its geophysical causes, which are the thermosteric expansion of the ocean water due to ocean warming, and ocean mass addition mainly due to land ice, ice shelf, and glacier melting [*Bamber et al.*, 2007; *Rignot et al.*, 2008; *Chen et al.*, 2009]. The upper ocean (0–700 m) warming and its thermosteric rise can be estimated from in situ measurements of ocean temperature profiles. These in situ measurements include using conductivity, temperature and depth (CTD) sensors, expendable bathythermographs (XBT), and Argo floats (Argo), which give a rate of 1.2 ± 0.8 mm/yr for the same period [*Willis et al.*, 2004, 2008, 2009; *Ishii and Kimoto*, 2009]. In addition, the Gravity Recovery and Climate Experiment (GRACE) data infer an ocean mass change of 0.85 ± 0.5 mm/yr over 2002–2008, after corrected by a glacial isostatic adjustment (GIA) model [*Paulson et al.*, 2007]. Although the GRACE record is 10 years shorter than the altimetry period, several studies have examined the issue of closing the sea level budget, i.e., the altimeter-observed SLR should match the sum of the steric sea level (SSL) and the ocean mass changes [*Lombard et al.*, 2007; *Willis et al.*, 2008; *Leuliette and Miller*, 2009; *Cazenave et al.*, 2009]. Particularly, *Leuliette and Miller* [2009] showed that the sea level budget could be closed to the range of data errors. However, their studies only apply to the GRACE period from 2003 to 2007, and it is still unclear whether their conclusion holds for the entire altimetry period. In addition, CTD/XBT/Argo only measures upper ocean temperature profiles; therefore, the steric

[1] Jet Propulsion Laboratory, California Institute of Technology, Pasadena, California, USA.
[2] CSIRO Marine and Atmospheric Research, Aspendale, Victoria, Australia.

0148-0227/11/2010JC006601

contribution from deep oceans has not been accounted for in those studies.

[3] Recent observational surveys have shown significant oceanic bottom water warming. For example, *Johnson et al.* [2007, 2008a, 2008b], *Meredith et al.* [2008], and *Purkey and Johnson* [2010] have shown that abyssal oceans are warming. Most interestingly, *Masuda et al.* [2010] demonstrated a mechanism of fast teleconnection between changes in the surface air-sea heat flux off the Adilie Coast of Antarctica and the bottom water warming in the North Pacific by moving the ocean representation backward in time with a 4-D data assimilation system. In contrast to the conventional estimates of a multicentennial timescale, they have shown that the connection can be established over only a few decades through the action of internal and topographic waves. However, in situ observations in deep oceans are spatially and temporally sporadic. It is still impossible to get an accurate estimate of the full depth steric height and ocean heat content from data alone. In addition, less attention has been given in quantifying the regional sea level changes and ocean heat content, even though departures from the global mean SLR could reach several decimeters in some regional areas. For example, it is shown that the mean sea level over the South China Sea has a rise rate of 11.3 mm/yr during 1993–2000 and a fall rate of 11.8 mm/yr during 2001–2005 [*Cheng and Qi*, 2007]. For the northeast coast of the United States, a collection of model projections have shown a rapid SLR in the next century, and the rise could have a greater effect on the heavily populated coastal regions than estimated previously [*Yin et al.*, 2009]. A recent review has concluded that improving estimates of the spatial variability in future sea level changes should be an important research target in coming years [*Milne et al.*, 2009].

[4] Ocean models have been the primary tools in quantifying sea level changes and project the 21st century sea level rise as well as estimate ocean heat content [*Wunsch et al.*, 2007; *Yin et al.*, 2009; *Gregory et al.*, 2004]. However, most of these ocean models are designed to conserve volume rather than mass [e.g., *Haidvogel and Beckmann*, 1999]. The volume conservation is imposed upon the ocean model by applying the Boussinesq approximation, which consists of the following three assumptions: (1) assuming a volume conservation law in the continuity equation, (2) replacing the variable density by a mean density in the momentum equations, and (3) using geopotential depth in the equation of state. Under these approximations, a uniform heating from the surface would not cause sea level rise in a Boussinesq ocean model. *Greatbatch* [1994] first noticed the incapability of Boussinesq models to represent the thermosteric effect on sea level rise and as a consequence introduced a globally uniform correction (Boussinesq correction). However, the globally uniform correction does not necessarily work in representing regional seal level changes, which is the main topic of this study. Similar concerns about ocean bottom pressure (OBP) have also been raised by *Ponte* [1999] and *Greatbatch and Lu* [2001]. They have noted that in a Boussinesq ocean surface heating effectively induces a mass loss, thereby creating a negative bottom pressure anomaly, with no immediate increase in sea level. *Huang and Jin* [2002] argued that the Boussinesq approximation was inconsistent with either altimetry sea surface height (SSH) or GRACE OBP. Differently, *Losch et al.* [2004] argued that the non-Boussinesq effects were most likely negligible with respect to other model uncertainties. However, their study was based on a 4° coarse resolution ocean model and the conclusions were not drawn by being compared with data. Nevertheless, these studies and concerns have never been confirmed by the most recently available long-term records of altimetry and GRACE data.

[5] Satellite altimeters have been observing ocean volume changes for about 17 years [*Ablain et al.*, 2009], and GRACE data has been used to derive ocean mass changes for about 7 years [*Tapley et al.*, 2004]. In situ CTD/XBT/Argo measurements have been used to derive upper ocean thermosteric expansion and ocean heat content for an even longer period [*Ishii and Kimoto*, 2009; *Levitus et al.*, 2009]. Here we will assess these three data sets with focuses on their seasonal variability and regional trends. As will be shown later, the data assessment is necessary not only for a better understanding of data uncertainties and incompleteness, but also for identifying model deficiencies. Different from previous modeling studies, we will examine results from a non-Boussinesq terrain-following ocean general circulation model (OGCM) to avoid uncertainties involving Boussinesq approximations in representing sea level changes and its regional trends.

[6] The paper is organized as follows: In section 2, satellite observations and in situ data sets are assessed and documented to reveal the fact that significant gap and uncertainties remain in the sea level budget with respect to their global mean and regional trends over the altimetry period. In section 3, we describe the ocean model and compare model results with observations. In section 4, we will combine the model with the observational data to give the full depth ocean heat content and steric sea level. We suggest that a complete explanation of the altimetry SLR map is possible. We will then verify the model by available ocean bottom water measurements. A summary and discussions are given in section 5.

2. Sea Level, Ocean Mass, and Upper Ocean Steric Expansion

[7] Three data sets have been analyzed: the altimetry SSH, GRACE OBP, and in situ upper ocean SSL. The altimetry SSH anomaly is a merged product of TOPEX/Poseidon, Jason-1, ERS-1, and EVISAT, which is produced and distributed by AVISO as part of the SSALTO ground processing segment (http://www.aviso.oceanobs.com). We have used the 1/4° gridded data with delayed time processing procedures that include corrections of glacial isostatic adjustment (GIA), tide, and atmospheric pressure. The data consist of weekly averages from 1993 to 2008. Figure 1 gives the annual amplitude, phase, and regional trends of the altimetry SSH.

[8] Since 2002, GRACE has been providing monthly estimates of the Earth's gravity field on spatial scales of a few hundred kilometers [*Tapley et al.*, 2004]. On seasonal to interannual timescales, changes in the gravity field can be interpreted as changes in a thin layer of water covering the Earth. Over the oceans, this is equivalent to changes in OBP. The pressure at the ocean bottom is the sum of the atmospheric pressure and the weight per unit area of the water

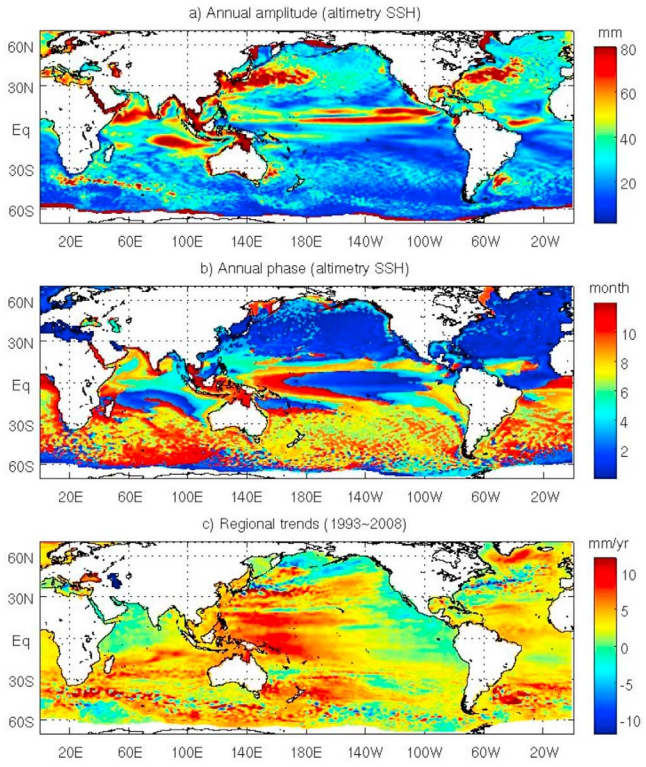

Figure 1. Altimetry SSH maps of (a) annual amplitude, (b) annual phase, and (c) trends from 1993 to 2008.

column, and can be approximately decomposed into three parts

$$p_b = p_a + \int_{-H}^{\eta^*} g\rho dz \approx p_a + g\rho_0\eta^* + \int_{-H}^{0} g\rho dz, \qquad (1)$$

here p_a is the atmospheric pressure, η^* is the sea level elevation, H is the ocean depth, g is the gravity coefficient, and ρ is ocean density. This equation reveals that the ocean bottom pressure is a combined contribution from atmospheric pressure, sea level, and water density.

[9] As the sea level responds to atmospheric pressure like an *inverted barometer* (ib), i.e., an increase in p_a of 1 mbar corresponds to a surface depression of approximately 1 cm, the barometric correction to the sea level

$$\eta^{ib} = -\frac{p_a}{g\rho_0} \qquad (2)$$

is often combined into the sea level. Substituting equation (2) into equation (1) and differentiating the equation with respect to time gives their anomaly relations

$$\frac{1}{g\rho_0}\frac{\partial p_b}{\partial t} = \frac{\partial(\eta^* - \eta^{ib})}{\partial t} - \left(-\frac{1}{\rho_0}\int_{-H}^{0}\frac{\partial\rho}{\partial t}dz\right). \qquad (3)$$

Equation (3) reveals that the ocean bottom pressure change is the contribution from the fluctuations of the barometrically corrected sea level and water density, a difference of two large terms. The term involving the density is referred to as the steric effect because changes in SSL are caused by changes in the density of the ocean column, implying an expansion or contraction of the column

$$SSL = -\frac{1}{\rho_0}\int_{-H}^{0}\frac{\partial\rho}{\partial t}dz. \qquad (4)$$

For convenience, OBP often translates to the thickness of water (i.e., OBP = $p_b/g\rho_0$). In this way, the OBP would have the same dimension as SSH in meters. Without particular indication, hereafter, we will refer to the OBP as the normalized pressure in centimeters of water. For its applications to ocean dynamics, we refer to *Song and Zlotnicki* [2008] and *Zlotnicki et al.* [2007]. We also refer to the barometrically corrected sea level as SSH, i.e., $\eta = \eta^* - \eta^{ib}$, which is the data shown in Figure 1.

[10] We use GRACE OBP data from *Chambers* [2008]. The data are processed from the most recent GRACE gravity field solutions (Release-04 from JPL and GFZ, and Release-04.1 from CSR), and publicly available from the GRACE web site (http://gracetellus.jpl.nasa.gov). This data set includes both atmospheric and nontidal oceanic pressure, which is consistent with equations (1)–(3). At the time this paper was written, the GRACE mission had released 75 months of data between April 2002 and December 2008 (with discontinuous a few months of missing data). These monthly OBP are equivalent water thickness values on a 1° grid with three different smoothing radiuses of 250, 500, and 750 km. They act as to reduce the short wavelength errors and remove the north-south strips in the GRACE gravity field solutions. We have used the data with the

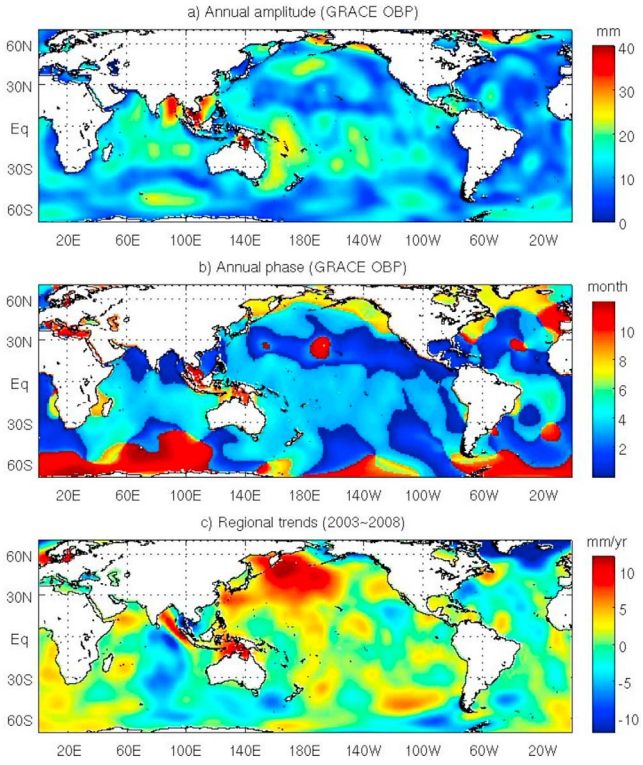

Figure 2. GRACE OBP maps of (a) annual amplitude, (b) annual phase, and (c) trends from 2003 to 2008.

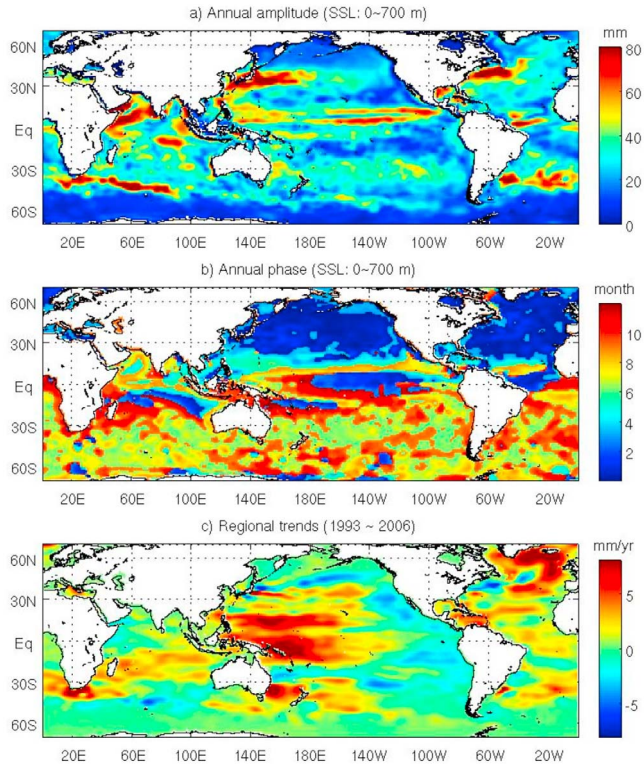

Figure 3. Upper ocean SSL maps of (a) annual amplitude, (b) annual phase, and (c) trends from 1993 to 2006.

smoothing radius of 500 km from the CSR release. Figure 2 shows the maps of the OBP annual amplitude, annual phase, and regional trends over the period of 2003~2008.

[11] It is important to point out that changes in gravity also reflect changes in the solid Earth such as Postglacial Rebound and even lithospheric redistribution after major earthquakes [*Han et al.*, 2006]. The GRACE mass estimates have a number of complications that contribute to their uncertainty. These include the sampling of nearby land signal along the coasts [*Guo et al.*, 2010] and the presence of correlated errors in the GRACE solutions [*Swenson and Wahr*, 2006; *Duan et al.*, 2009], and geocenter motion errors [*Swenson et al.*, 2008]. In summary, large uncertainties in GRACE data remain. These uncertainties are found in both global and regional scales. Because this reason, we only use the global mean of the GRACE data to infer ocean mass gain. Its spatial distribution is not used in our calculations, but serves for comparison with the ocean model fields.

[12] When comparing the OBP maps (Figure 2) with the corresponding SSH maps (Figure 1), we notice that they are quite different. First, most of the seasonal variability in SSH (Figure 1a) is related to the major oceanic circulation features, such as the Gulfstream and Kuroshio extensions and the equatorial current system, while the OBP (Figure 2a) has little signature of them. Second, there are strong coastal OBP features in marginal seas and coastal oceans (Figure 2a), which may be related to the land hydrology signals that leak into the ocean grid. This may be a consequence of applying smoothing filters during the data processing [*Swenson and Wahr*, 2006]. Finally, the high OBP values in the Bay of Bengal of the Indian Ocean, particularly in the trend map are a result of seafloor motions of the 2004 Andaman-Sumatra earthquake, which has been studied by *Han et al.* [2006] and *Song and Han* [2011].

[13] We have also examined upper ocean (0–700 m) SSL data from *Ishii and Kimoto* [2009] and *Kuo et al.* [2008]. This data set consists of monthly 1° grid maps from January 1945 to December 2006. Figure 3 displays the maps of annual amplitude, phase, and regional trend of the SSL over the period of 1993–2006. The SSL annual amplitude and phase (Figures 3a and 3b) are almost identical to the corresponding SSH patterns (Figures 1a and 1b), suggesting that the seasonal SSH variability is largely explained by the upper ocean thermosteric expansion. This similarity suggests that surface heat is essentially stored above the seasonal thermocline, thereby producing the near-surface steric changes in sea level. However, their regional trends are quiet different, although there are similarities in the western Pacific and northern Atlantic. In general, the regional trends in the upper ocean SSL are much weaker than in the SSH trends. This is also true for the period of 2003–2006 when all three data sets are available (not shown). The discrepancies in regional trends suggest that a significant source or cause to the present-day SLR is missing. This is the main issue to be discussed in this paper.

[14] To gain insight into the discrepancy among these three data sets, particularly, in their trend maps, we rewrite equation (3) into the sea level change equation and divided into four variables. The three variables in the right are the geophysical causes of the sea level change

$$\frac{\partial \eta}{\partial t} = \left(-\frac{1}{\rho_0} \int_{-700\,\mathrm{m}}^{0} \frac{\partial \rho}{\partial t} dz - \frac{1}{\rho_0} \int_{-H}^{-700\,\mathrm{m}} \frac{\partial \rho}{\partial t} dz \right) + \frac{1}{g\rho_0} \frac{\partial p_b}{\partial t}. \quad (5)$$

The total in the brackets is the full depth SSL and has been divided at 700 m into upper ocean (0–700 m) and deep ocean (below 700 m) contributions, to be consistent with available upper ocean data of *Levitus et al.* [2009] and *Ishii and Kimoto* [2009]. The sea level closure equation (5) suggests that SLR is the combined contribution from steric expansion due to full depth ocean warming and ocean mass gain due to mainly freshwater addition. Notice that altimetry SSH, GRACE ocean mass, and in situ upper ocean SSL data represent only three of the four variables in the closure equation. The contribution from deep oceans has not been accounted for.

[15] Figure 4a compares the time series of these three variables for their global (65°S–65°N) means. Since GRACE is only available after 2003 we have used *Domingues et al.*'s [2008] ocean mass estimate from glacier and ice cap contributions (the heavy red line), which gives a global mean SLR of 0.8 ± 0.2 mm/yr over 1993–2003. For the GRACE period of 2003–2008, a rate of 0.85 ± 0.5 mm/yr is used, consistent with *Willis et al.* [2008] and *Leuliette and Miller* [2009]. These two estimates suggest that the global ocean mass has been increased by about 0.85 mm/yr over 1993–2008 (thin black line). Because we don't have the Ishii upper ocean SSL after 2006, we have projected the trend for 2007–2008 the same as the previous years, which gives a rate of 1.2 ± 0.8 mm/yr (thin blue line). Figure 4b compares the altimetry SSH with the sum of the upper ocean SSL and the GRACE ocean mass. It can be seen that the upper ocean SSL

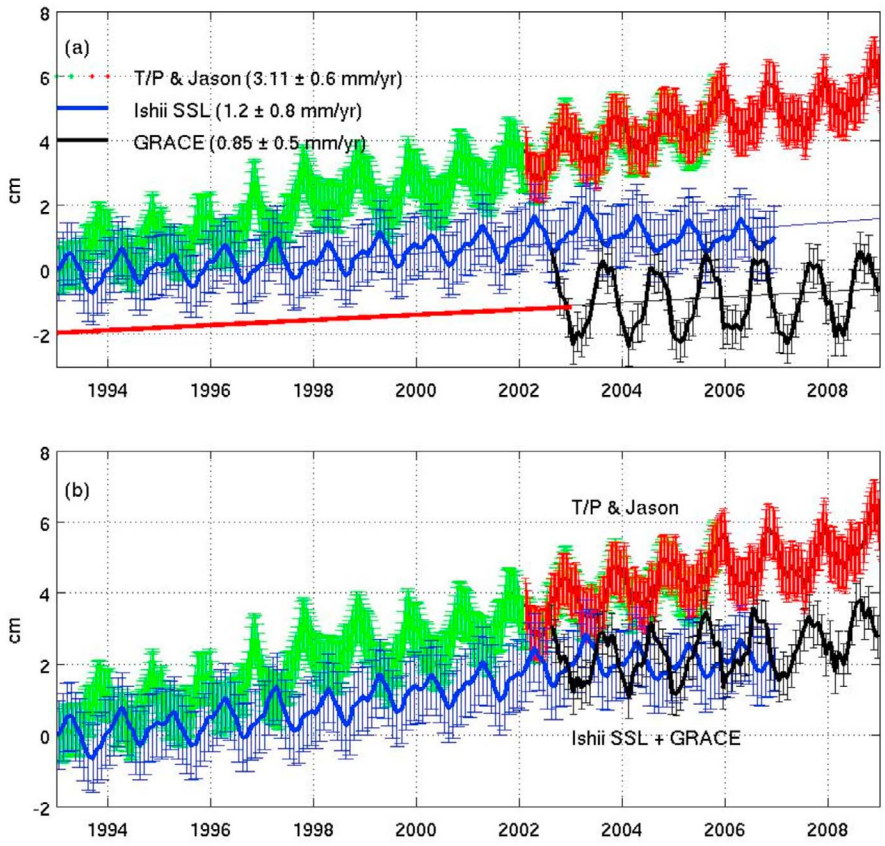

Figure 4. (a) Time series of altimetry SSH, GRACE ocean mass, and upper ocean (0–700 m) SSL from *Ishii and Kimoto* [2009], averaged over global ocean (65°S–65°N). The heavy red line before 2003 is the estimated ocean mass with a trend of 0.8 mm/yr from *Domingues et al.* [2008]. (b) Comparison of the altimetry SSH with the combined upper ocean SSL and GRACE ocean mass.

trend when added onto the GRACE trend does not match the altimetry trend of the SLR even with taking their error bars into consideration.

[16] In summary, we can conclude the following from the data assessment:

[17] 1. The seasonal variability of altimetry SSH (Figures 1a and 1b) can be explained quite well by the in situ upper ocean steric height (Figures 3a and 3b), suggesting that surface heat is essentially stored above the seasonal thermocline, thereby producing the near surface steric changes in sea level. No significant contribution from deep oceans is needed to close the sea level budget in its annual amplitude and phase maps.

[18] 2. Differently, the altimetry SSH trend map (Figure 1c) cannot be explained by the sum of the in situ upper ocean SSL and the GRACE ocean mass (Figures 2c and 3c). This is also true for the period of 2003–2006 when all three data sets are available. Note that this conclusion does not necessarily conflict with *Leuliette and Miller* [2009] or *Cazenave et al.* [2009] because they only compared the global means over 2003–2007.

[19] 3. In addition, the global mean SLR of 3.11 mm/yr from altimeters does not match the upper ocean SSL rate of 1.2 mm/yr plus the GRACE trend of 0.85 mm/yr (Figure 4b) over the altimetry period, leaving one-third of the altimetry SLR unexplained.

[20] It should be noted that previous studies on the sea level budget closure only consider the global mean time series for a short period of time from 2003 to 2007. For example, *Lombard et al.* [2007] found a strong discrepancy between altimetry minus GRACE and in situ based steric sea level trend over 2003–2005 and related the discrepancy to inadequate sampling of in situ measurements. The inadequate sampling was later confirmed in large part to a set of systematic errors in the Argo data [*Willis et al.*, 2009]. After the systematic errors corrected, *Willis et al.* [2008] still found a discrepancy of 3.3 mm/yr between 2003 and 2008 and suggested systematic long-period errors in one or more of these observing system. With slightly better Argo coverage over the period 2004–2008, *Leuliette and Miller* [2009] shown that the sea level budget can be closed within the range of error bars for both phase and amplitude. Figure 4b shows that such a closure is possible for the short period of their studied, but the gap widens beyond the error bars if considering the entire altimetry period from 1993 to 2008. Another issue is that these studies applied the glacial isostatic adjustment (GIA) correction over the ocean using the *Paulson et al.* [2007] model, which increases the trend

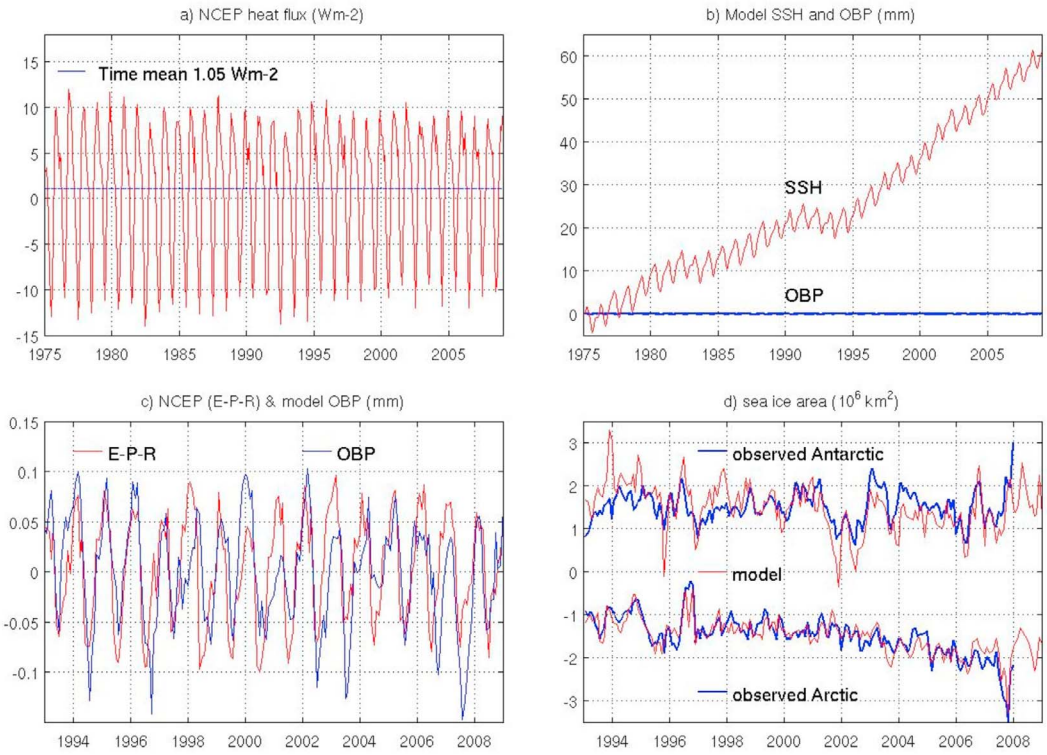

Figure 5. Model calibration: (a) globally averaged surface heat flux and its time mean, (b) model SSH and OBP, (c) zoom in the model OBP and corresponding surface freshwater flux (E-P-R, evaporation minus precipitation and restoring to sea surface salinity data), and (d) sea ice area observations and corresponding model results for both polar regions (seasonal cycles removed).

of observed ocean mass variations by 1 mm/yr. However, *Cazenave et al.* [2009] further improved the budget closure by reproducing GRACE estimate but with a different GIA model, the ICE-5G (VM4) model [*Peltier*, 2004], which gives a much larger rate of 1.9 mm/yr in ocean mass change. *Peltier* [2009] has a similar budget closure result as *Cazenave et al.* [2009]. More recently, *Wu et al.* [2010] simultaneously estimated the present-day water transport and GIA, which gives a global nonsteric mean sea level rise (or ocean mass change) of only 0.54 ± 0.3 mm/yr. The inconsistency of the GRACE ocean mass estimates between these studies is clearly a big problem. In the following, we will take a different approach to the sea level budget issue by focusing on diagnosing the deep ocean steric height from a non-Boussinesq ocean model.

3. Non-Boussinesq Terrain-Following Coordinate OGCM

[21] Our non-Boussinesq ocean general circulation model (OGCM), based on *Song and Hou* [2006] and *Song et al.* [2011], is an evolving version of ROMS [*Shchepetkin and McWilliams*, 2005] (http://www.myroms.org). It has a 1/4° horizontal resolution and is coupled to a sea ice model [*Budgell*, 2005]. The major feature of the non-Boussinesq model is the stretched pressure coordinate (*sp* coordinate) system that allows both terrain-following coordinate feature [*Song and Haidvogel*, 1994] and non-Boussinesq approximations of the seawater. Both polar regions are included with the northern pole shifted toward the Russian continent. The water depth of the model is divided into 30 terrain-following levels. The shallowest water is 20 m and the deepest water sets 5500 m, and the topography data is from ETOPO2. The model is spun-up for 30 years with the NCEP/NCAR monthly climatology [*Kalnay et al.*, 1996] to reach an approximately steady state and is then driven by daily NCEP/NCAR reanalysis forcing from 1990 to 2008. The surface heat flux is corrected by the daily sea surface temperature (SST) data and the surface salt flux is corrected by the sea surface salinity climatology [*Barnier et al.*, 1995; *Conkright et al.*, 2002]. No water mass from land-based water is added to the ocean, but the evaporation minus precipitation (E-P) distribution is still applied and corrected by river runoff climatology, such that the freshwater flux has insignificant contribution to the sea level. For simplicity, we call this part of freshwater flux as E-P-R, standing for the evaporation minus precipitation (E-P) distribution and the climatology restoration.

3.1. Model Calibration

[22] Before comparing the model with observations, we have first calibrated the model for the following aspects. Figure 5 summarizes these calibrations.

3.1.1. Heat Flux Consistency

[23] Figure 5a gives the surface heat flux of the model. Although the seasonal heat flux varies dramatically, it has a

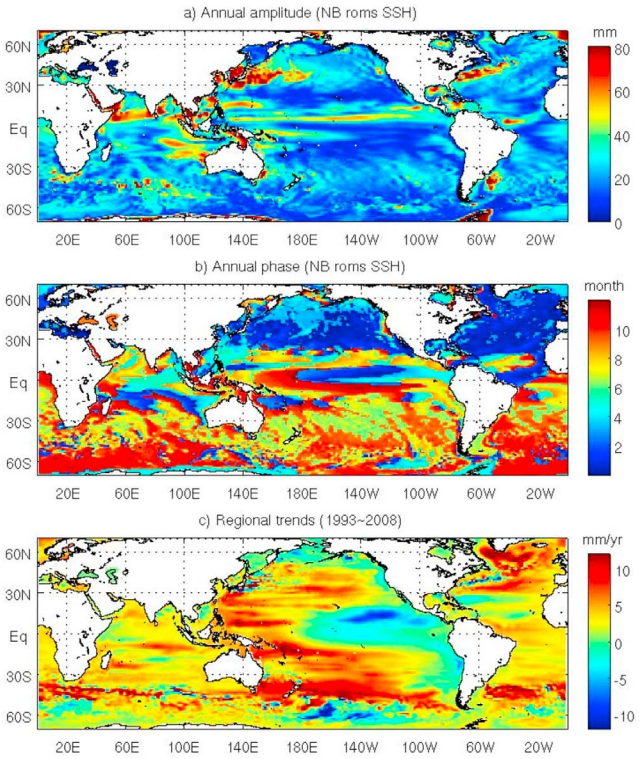

Figure 6. Model SSH maps of (a) annual amplitude, (b) annual phase, and (c) trends from 1993 to 2008. NB, non-Boussinesq approximations.

positive global mean of 1.05 Wm^{-2} averaged over the entire surface of the Earth or 1.45 Wm^{-2} averaged over the surface of the global ocean, indicating the ocean gains heat from atmosphere. The model heat flux is consistent with the observed increasing concentrations of carbon dioxide and other greenhouse gases that lead to an imbalance at the top of atmosphere (TOA) of 0.9 ± 0.5 W m^{-2} [*Trenberth and Fasullo*, 2010]. In the real ocean, surface heating causes sea level rise. This is true in our non-Boussinesq model, as shown in Figure 5b. The surface heat flux causes a total global SLR of 62 mm over 1975–2008 in the model, corresponding to a global SLR of 1.82 or 1.26 mm/yr per 1 Wm^{-2} heat flux averaged over the surface of the global ocean. This is consistent with *Wunsch et al.* [2007], who estimated that a heat flux of 1 Wm^{-2} would cause a global sea level rise of about 1.3 mm/yr. Note that the model SSH is essentially the steric height because no land-based water mass is added to the ocean.

3.1.2. Mass Conservation Consistency

[24] Figure 5b also gives the model OBP or ocean mass change, which is conserved and shows no drift in the 34 yearlong simulation. With no mass addition from land-based waster sources, the model should conserve mass. This is essentially true in our non-Boussinesq model. Figure 5c zooms in the OBP and compares it with model surface freshwater flux (E-P-R) for the period from 1993 to 2008. Note that the model has a small amount of freshwater flux. However, the model mass change is consistent with the freshwater flux in a very small range of 0.1 mm.

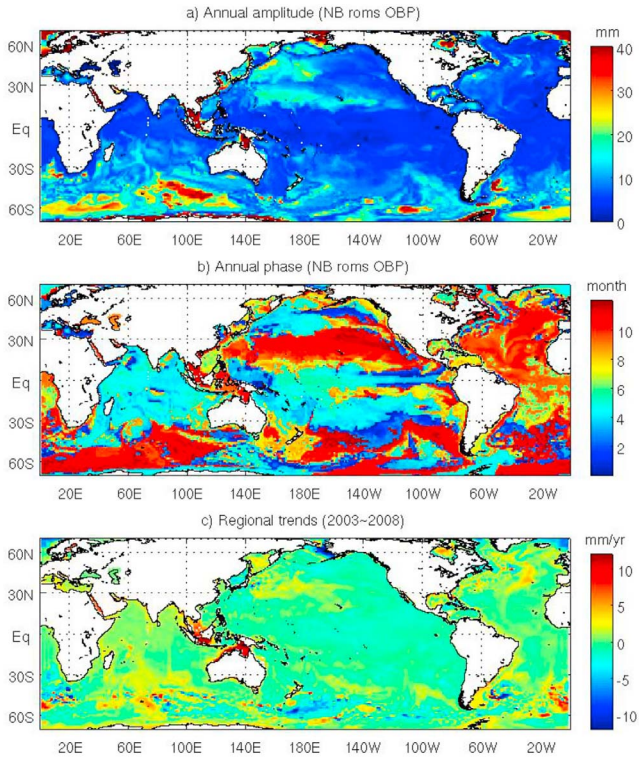

Figure 7. Model OBP maps of (a) annual amplitude, (b) annual phase, and (c) trends from 2003 to 2008.

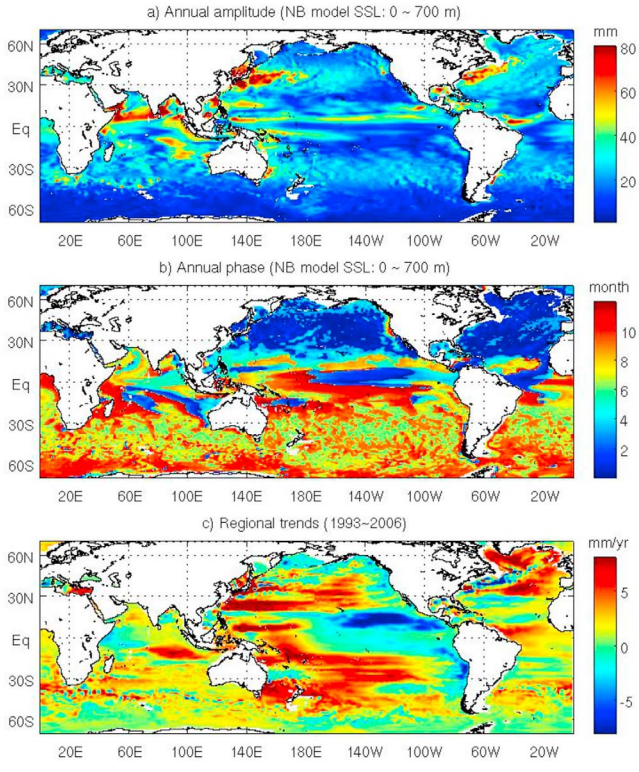

Figure 8. Model upper ocean (0~700 m) SSL maps of (a) annual amplitude, (b) annual phase, and (c) trends from 1993 to 2006.

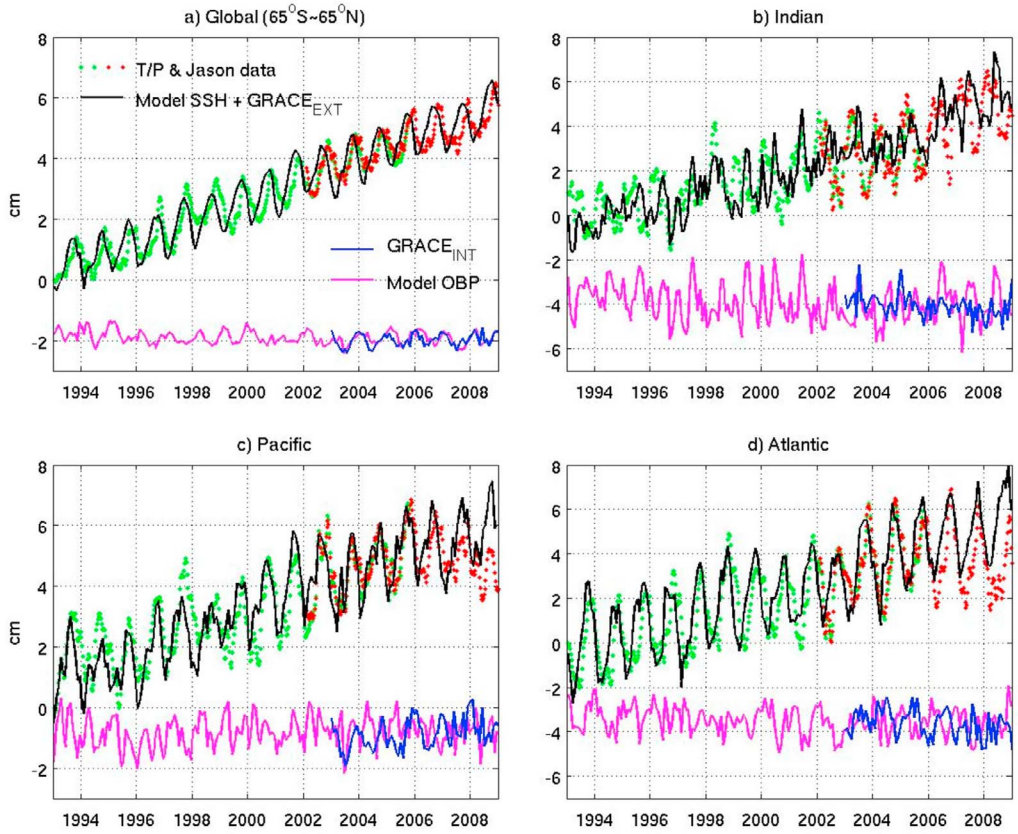

Figure 9. Time series of altimetry data (green and red dots), internal mass change from GRACE (blue curve), model SSH (black curve), and OBP (magenta curve). They are averaged over the (a) global ocean (65°S–65°N), (b) Indian Ocean, (c) Pacific Ocean, and (d) Atlantic Ocean. The global mean of GRACE ocean mass (external mass change) has been added to the model SSH to be consistent with altimetry data.

3.1.3. Sea Ice Extension Consistency

[25] We have also compared the sea ice areas with satellite observations because sea ice is believed to be sensitive to ocean warming. Figure 5d shows that the model agrees well with the satellite-observed sea ice extension from *SMMR* and *SSM/I* in both Arctic and Antarctic regions [*Stroeve and Meier*, 1999], suggesting that the ocean is neither over heating nor over cooling at least in its two polar regions. Next we focus on comparing the model with the three observational data sets that have been assessed earlier.

3.2. Comparison With Data

[26] Figure 6 gives the model SSH for comparison with altimetry SSH data, Figure 7 gives model OBP corresponding to the GRACE data, and Figure 8 give the model upper ocean (0–700 m) SSL for comparison with *Ishii and Kimoto* [2009] SSL data. First, the model SSH agrees well with the altimetry SSH in both annual amplitude and phase maps (Figures 1a and 1b). However, the model trends show significant cooling in the eastern tropical Pacific (Figure 6c), which is not seen in the altimetry data (Figure 1c). This typical cold bias is observed in many coupled climate models but may also be caused by the NCEP/NCAR forcing which has insufficient grid resolution in the tropical oceans. Second, the modeled OBP (Figure 7) differs from the GRACE OBP (Figure 2) in intensity, phase, and most predominantly, in trends. The reason for the differences seen in the trends may be a consequence of seafloor motions that have been observed by GRACE, but not included in the model simulation. In addition, GRACE data represents both mass additions from land and internal ocean mass changes, while the model does not include land-based water sources. Third, the model upper ocean (0–700 m) SSL (Figure 8) compares favorably to *Ishii and Kimoto* [2009] data (Figure 3) for the annual amplitude and phase maps, but less so for the trends. Nevertheless, seasonal variability of the model SSH is explained well by the model upper ocean SSL. This is consistent with our earlier data assessment that the seasonal variability of altimetry SSH can be explained well by the in situ upper ocean SSL.

[27] Figure 9 compares times series of model SSH and OBP with altimetry and GRACE data in both global means and basin averages. In order to allow for a meaningful comparison between model and observation, we have to deal with the issue that the model does not have the ocean mass from land-based water sources (the *external mass*). Thus, the model only estimates internal mass changes, including effects of evaporation, precipitation, and restoring terms (E-P-R). GRACE data on the other hand contains both, internal and external mass changes and hence is not

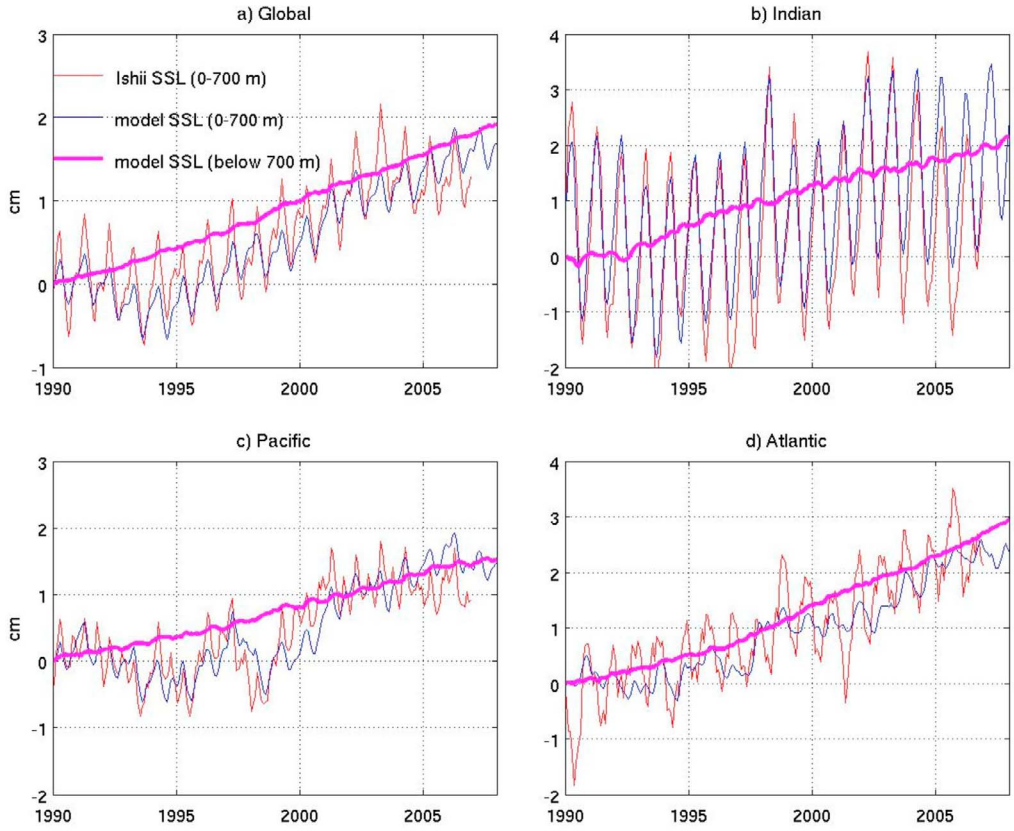

Figure 10. Time series of in situ upper ocean (0–700 m) SSL (red curve), corresponding model upper ocean (0–700 m) SSL (blue curve), and model deep ocean (below 700 m) SSL (thick magenta curve). They are averaged over the (a) global ocean, (b) Indian Ocean, (c) Pacific Ocean, and (d) Atlantic Ocean.

comparable to model values per se. To correct this discrepancy, we make use of the fact that the globally averaged GRACE ocean mass change is equivalent to the external mass added from land sources. Equivalently this means that the global averaged mass change as calculated by the model is zero (this is true as shown in Figure 5b). Consequently, GRACE internal mass changes can be calculated simply by removing its global mean. This allows for comparing model OBP with the internal GRACE OBP. A similar argument is made for the model SSH, which does not include external mass input from land sources, but altimetry data do. In order to compare model values with observations we add the GRACE global mean (external mass change) to the model SSH (internal mass change). For the years that are not covered by GRACE an ocean mass trend of 0.85 mm/yr has been assumed [*Domingues et al.*, 2008], and has been added to the modeled SSH. Figure 9 compares the time series of model (total) SSH and OBP with altimeter SSH and GRACE internal mass changes. The comparison suggests some phase lags (1~2 months) in the global and Atlantic averages of SSH, indicating errors in the model or in GRACE which may be related to land signal leakages into the ocean. In general, the model agrees well with the altimetry SSH and GRACE in their global means and basin averages.

[28] The time series of modeled upper ocean (0–700 m) and deep ocean (below 700 m) SSL are shown in Figure 10, and are compared with in situ upper ocean SSL of *Ishii and Kimoto* [2009]. First of all, we notice that the time series of the deep ocean steric heights have very little annual and interannual signals. However, their warming trends are significant; in fact, they are slightly higher than those of the upper oceans, with rates of 1.1, 1.3, 1.0, and 1.4 mm/yr for the global ocean and locally for the Indian, Pacific, and Atlantic Ocean, respectively. The observed deep ocean warming will be discussed in more detail in section 4. The upper ocean model-data comparison shows that the model results are consistent with data from *Ishii and Kimoto* [2009], except for a positive bias that becomes apparent after 2004. It is unclear whether this bias is due to the insufficient correction of the instrument bias [*Willis et al.*, 2008] or due to NCEP/NCAR reanalysis used to force the model.

[29] To further investigate the differences, we have also calculated the model heat content and compared it with *Levitus et al.* [2009] in Figure 11. The upper ocean (0–700 m) heat content is calculated using

$$HC(t) = \iint_A C_p \left\{ \int_{-700\,\mathrm{m}}^{0} T(t)\rho(t)dz \right\} dA, \qquad (6)$$

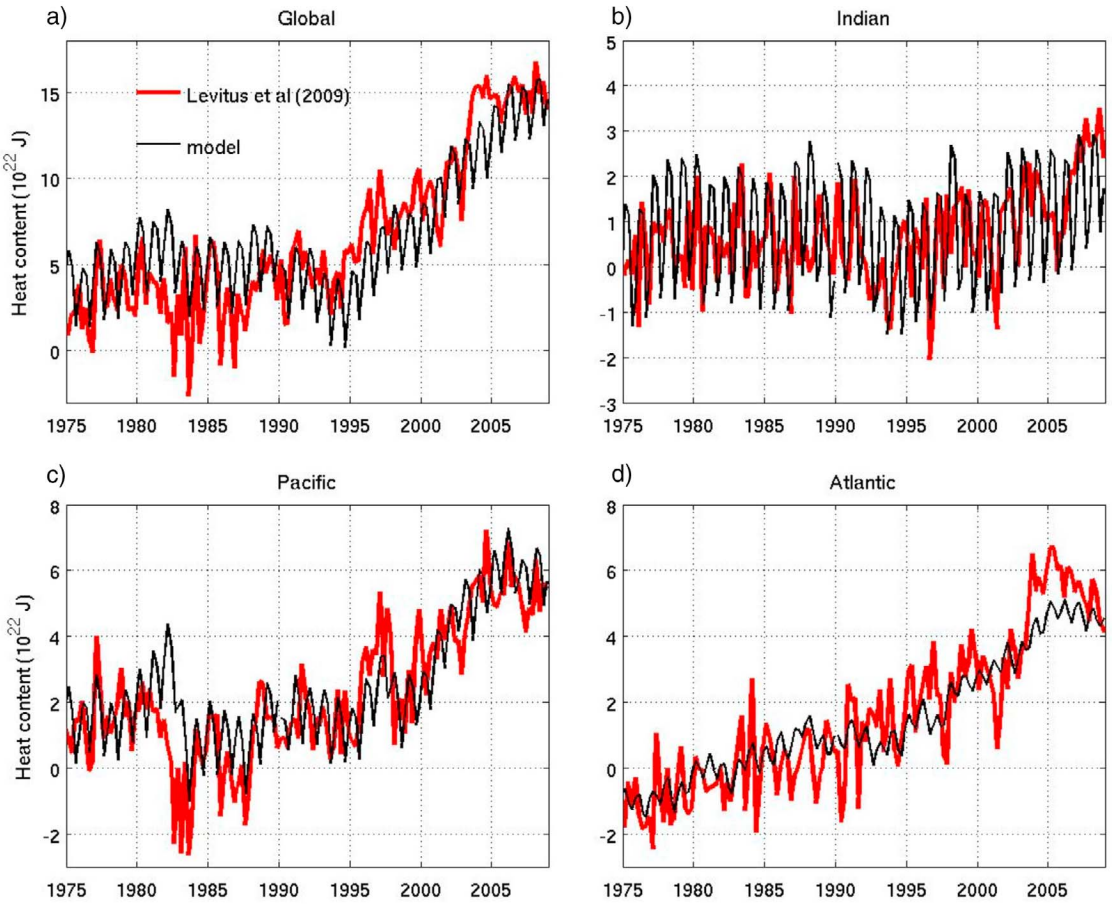

Figure 11. Time series of in situ upper ocean (0–700 m) heat content (red curve) and corresponding model results (black curve). They are averaged over the (a) global ocean, (b) Indian Ocean, (c) Pacific Ocean, and (d) Atlantic Ocean. All time series are seasonally averaged (every 3 months).

where t is time, $T(t)$ and $\rho(t)$ are the ocean temperature and density field, A is the ocean area, and C_p (=3990 J/kg/C) is the heat capacity. The 700 m depth is chosen in order to be consistent with the available upper ocean data. Figure 11 shows that the model is consistent with the upper ocean heat content in both global and basin averages. However, differences between their annual amplitudes are apparent. In the Indian Ocean, the model shows the largest annually cycle. Observations compare well with the seasonal cycle before 2003 but start to deviate from the mean thereafter. For the Atlantic Ocean the model amplitude of the seasonal cycle is smaller than those of the observations. These differences may indicate model deficiencies in resolving the heat transport between these two oceans, even though their global means and Pacific basin averages compare fairly well.

4. Comparison With Bottom Water Measurements and Altimetry SLR Map

[30] So far, we have mostly assessed the upper ocean (0–700 m) data, satellite SSH and OBP data, and compared them with the model. In this section we focus our attention on the deep ocean. Figure 12 shows the model deep ocean SSL below 700 m. Note that the seasonal variability in the deep ocean SSL is rather weak, particularly for the annual amplitude. This is consistent with the previous data assessment, suggesting that deep oceans contribute very little to the seasonal variability of the sea level. However, the story is different for the regional trends. The model suggests a significant deep ocean warming trend, particularly in the North Atlantic and along the Antarctic Circumpolar Current (ACC). The warming features appear closely related to the oceanic circulation and dynamics. As such they may provide an explanation as to why altimetry SLR cannot be adequately explained by the sum of upper ocean (0–700 m) SSL and ocean mass change calculated from GRACE (discussed in section 3).

[31] In order to verify a possible hypothesis that connects the deep ocean warming to the missing part of the sea level budget closure, the following two conditions should be fulfilled: (1) The model deep ocean warming should be consistent with available bottom water measurements, and (2) its combination with the in situ upper ocean SSL and GRACE data should explain the altimetry SLR in both global mean and regional trends. In the following we discuss these two conditions in more detail.

4.1. Comparison With Bottom Water Measurements

[32] We have compared the model with two sets of ocean bottom water measurements. The first data set is from

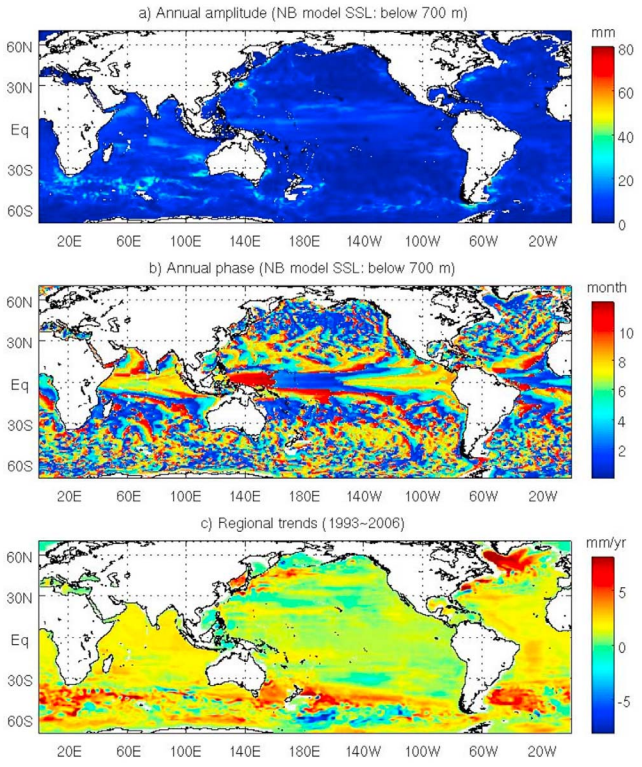

Figure 12. Model deep ocean (below 700 m) SSL maps of (a) annual amplitude, (b) annual phase, and (c) trends from 1993 to 2006.

Johnson et al. [2007, 2008a, 2008b]. They suggested that deep oceans below 2000 m along several sections had warmed since 1990. In Figure 13, we show the model temperature trends below 2000 m, as well as along-section-averaged temperature change profiles. These profiles correspond to those of *Johnson et al.* [2007, 2008a, 2008b]. First, we notice that the deep ocean warming is unevenly distributed among the abyssal basins with the Atlantic Ocean experiencing the strongest warming, the Indian Ocean the second warmest, and the Pacific Ocean the least (Figure 13a). This agrees with the basin-averaged in situ upper ocean SSL data in Figure 10. Figures 13b–13e compare the model temperature change profiles with the measurements of *Johnson et al.* [2007, 2008a, 2008b]. The section-averaged profiles generally suggest that the Atlantic and Indian sections have warmed faster than the Pacific sections. This uneven basin-to-basin warming is also evident in observational data. For example, in the Indian Ocean, *Johnson et al.* [2008a] show a temperature rise of about 0.05–0.1°C has been taken place between 1995 and 2007. The model gives a similar temperature profile rise in the range of 0~0.07°C for that section (Figure 13b). In the Pacific, *Johnson et al.* [2007] show warming of 0.008°C has occurred between 1991 and 2006 on the north-south section (0.01°C between 1992 and 2003 in the east-west section). The corresponding model profiles give values within −0.01~0.02°C for these sections (Figures 13c and 13d). In the Atlantic Ocean, *Johnson et al.* [2008b] show a section temperature profile with a maximum warming of 0.13°C near 5000 m depth between 1983 and 2003. Our model shows a similar maximum warming of 0.13°C, but is located at a depth of 3000 m between 1990 and 2008 (Figure 13e). This middepth warming might be associated with changes in the North Atlantic Deep Water as shown by *Johnson and Doney* [2006] that a bottom-intensified warming signal in the South Atlantic linked with the Antarctic Bottom Water. Nevertheless, the model reproduces those main features of the observations.

[33] Next we compare the model with *Purkey and Johnson* [2010] with focus on the oceanic bottom water warming and its contribution to SLR. *Purkey and Johnson* [2010] use topographic features to divide the globe into 32 abyssal basins, as shown in Figure 14a, and estimated a deep temperature trend for each of these abyssal basins using measurements along 28 full depth and high-quality hydrographic sections over the period 1981–2010. They also calculated basin means of SLR due to abyssal thermal expansion below 4000 m from the bottom water surveys, which has been reproduced in Figure 14a. We have also calculated the local SLR, as shown in Figure 14b. Note that the local SLR is not necessarily uniformly distributed in an arbitrary abyssal basin as estimated by *Purkey and Johnson* [2010] from the limited numbers of observations. To have a meaningful comparison, we will first compare their geographic distributions of local SLR trends, and then their global averages with model values. The model agrees remarkable well with the geographic distributions of warming and cooling trends from the bottom water surveys in the 32 abyssal basins. For example, toward the west of the Mid-Atlantic Ridge the South Atlantic Ocean exhibits a north-south-oriented tripole with large warming trends surrounding a smaller area of cooling. To the east of the Mid-Atlantic Ridge cooling trends are rather dominant. These patterns are mostly consistent with observed trends of warming or cooling. The Indian Ocean consists of several small abyssal basins, which show a pattern of warming in the south and cooling in the north. This pattern is again consistent with the bottom water survey. In the Pacific Ocean, the model suggests cooling trends in most of the abyssal basins except for the subpolar basin in the North Pacific and to the east of New Zealand. This trend is not seen in the observations, suggesting some model deficiencies here. The model shows further cooling trends in the two abyssal basins off Antarctica corresponding to the eastern Indian Ocean and the eastern Pacific Ocean sector. We don't know what kind of physical mechanisms causes the cooling trends in these abyssal basins. Sensitivity study might give some clue, but it is beyond the scope of this study. Nevertheless, taken together the model gives a global mean SLR contribution of 0.018 mm/yr from all abyssal oceans below 4000 m over 1990–2000. This is less than the 0.053 ± 0.017 mm/yr estimated by Purkey and Johnson's for the period of 1990s–2000s, suggesting the model may underestimate bottom water warming in total. The averaged warming trend in the deep waters (1000~4000 m) south of the Sub-Antarctic Front (SAF, approximately at 40°S) exhibits the strongest warming trend corresponding to 0.11 mm/yr of global sea level rise. This is slightly higher than *Purkey and Johnson*'s [2010] rate of 0.093 ± 0.081 mm/yr over 1990s–2000s. Interestingly, the total contributions from the two parts (below 4000 m and 1000–4000 m south of the SAF) in

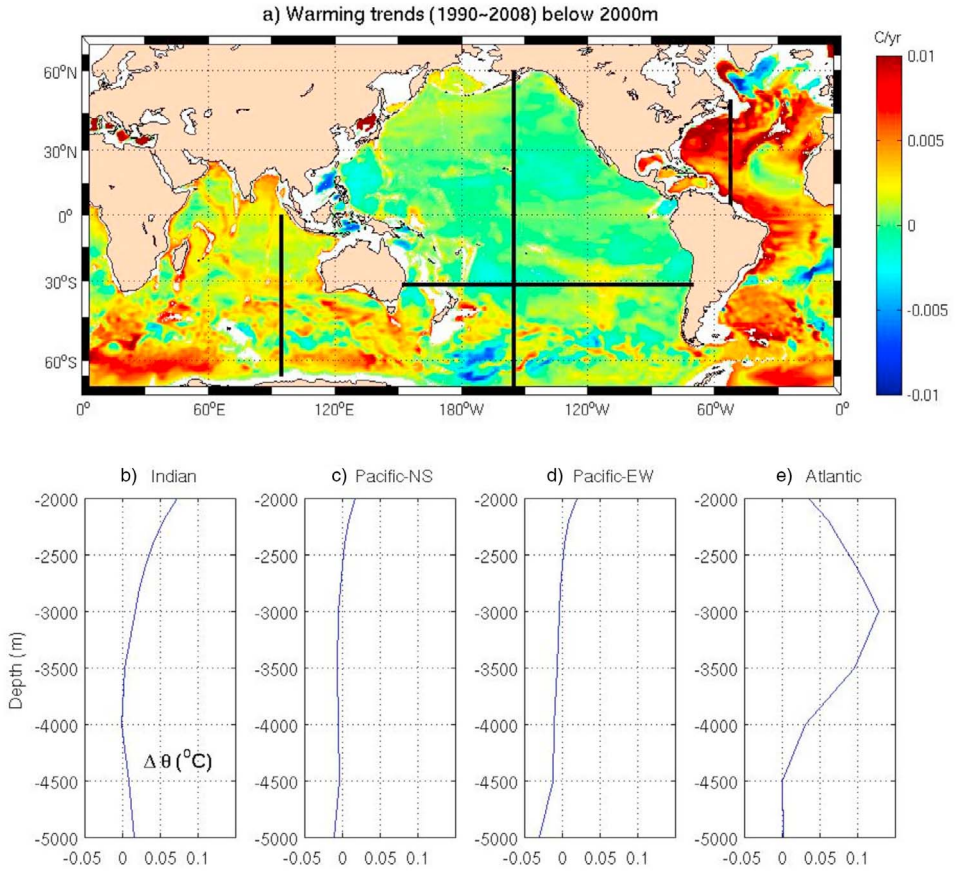

Figure 13. (a) Regional trends of model ocean temperature below 2000 m, and (b–e) temperature profile changes averaged along the corresponding sections marked by the heavy lines in Figure 13a, from 1990 to 2008.

the model are consistent with the estimate of *Purkey and Johnson* [2010]. The model also confirms their conclusion that deep water warming is mostly prominent in the Antarctic south of the Sub-Antarctic Front.

4.2. Comparison With Altimetry SLR Map

[34] Sea level trend map is another constrain of the deep ocean warming because the full depth steric height due to ocean warming, plus the ocean mass addition from land-based water sources, should explain the altimetry SLR map. Since our model appears consistent with the upper ocean (0–700 m) and bottom water (below 4000 m) steric heights (Figures 10–14), we can use the model as a proxy for an estimate of the full depth steric height due to ocean warming. For easy comparison, we have reproduced the altimetry SLR map in Figure 15a, while Figure 15b is the combination of the in situ upper ocean (0–700 m) SSL from *Ishii and Kimoto* [2009], deep ocean (below 700 m) SSL from model, and an additional external ocean mass trend of 0.85 mm/yr as suggested by *Domingues et al.* [2008] and GRACE data (see Figure 4a). The data-model combination explains the altimetry trend map quite well, except for the eddy features, which are not resolved by the in situ upper ocean SSL data. Furthermore, the combined SSH values in the subpolar region off Greenland are much higher than the altimetry data. This discrepancy is likely due to melting of Greenland glaciers, which has been measured by GRACE and reported by *Velicogna* [2009], but is not included in the model. Nevertheless, we obtain a global mean steric rise of 1.1 mm/yr from the model deep ocean warming below 700 m. Adding to the 1.2 ± 0.8 mm/yr from in situ upper ocean (0–700 m) SSL and about 0.85 ± 0.5 mm/yr from GRACE, the resulting sea level rise matches the altimetry SLR of 3.11 ± 0.6 mm/yr fairly well.

[35] It should be noted that about 82% of the ocean water is below 700 m if assuming a mean depth of 3800 m. Even if the deep ocean just warmed slightly, its contribution to the global SLR cannot be ignored because of its large volume. For the last 18 years, altimetry data have suggested that the global sea level has been raised with an accelerated rate. This is also true for the corresponding upper ocean SSL derived from in situ measurements. In fact, upper ocean heat content from *Levitus et al.* [2009] has shown an increase since 1955, despite some interannual variations. Such a long-term upper ocean warming would eventually affect deep oceans [*Masuda et al.*, 2010]. Bottom water measurements and our model simulation show a consistent warming rate since 1990s. We understand that recent Argo floats can

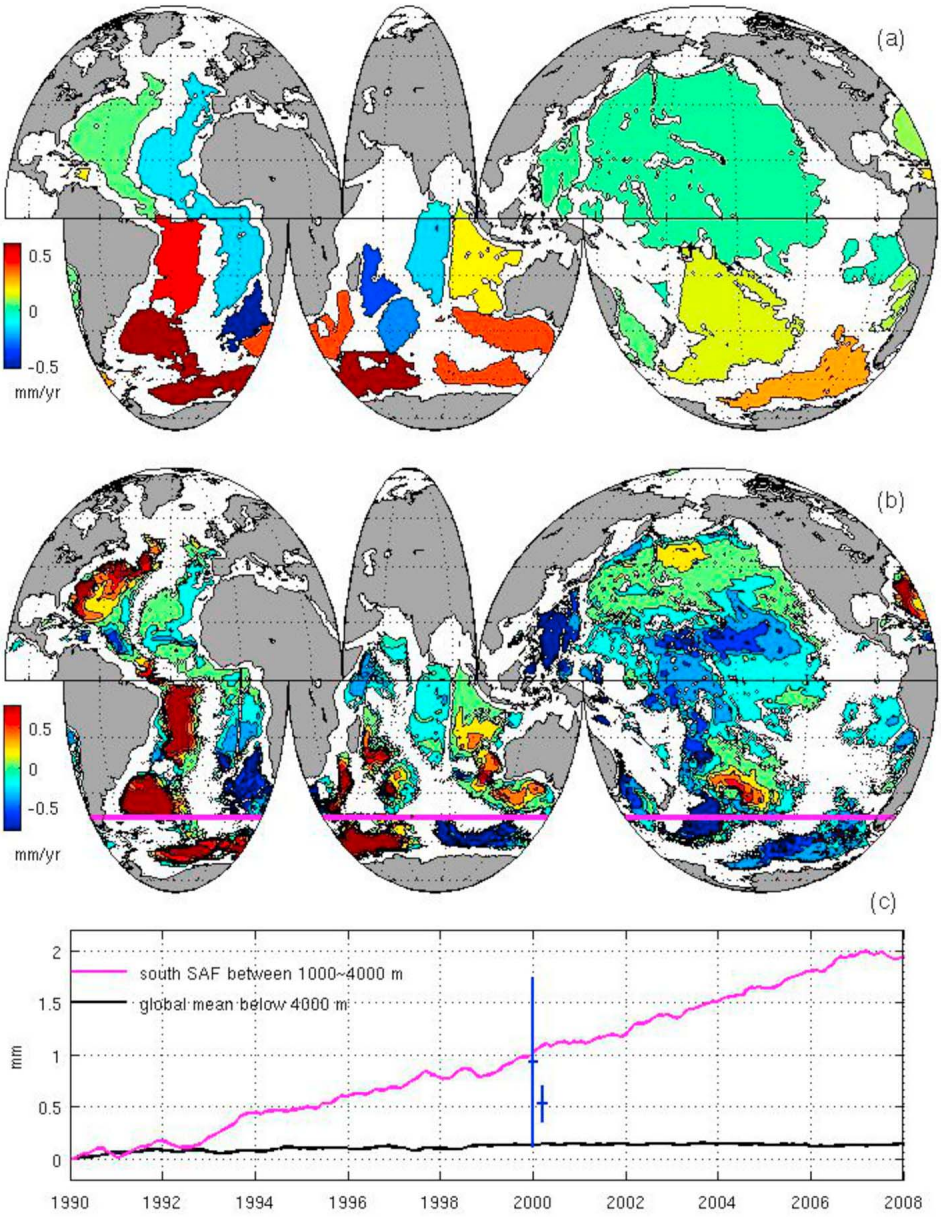

Figure 14. (a) Basin mean of SLR from the 1990s to the 2000s below 4000 m, reproduced from *Purkey and Johnson* [2010]. (b) Model local SLR map from 1990 to 2008 due to abyssal thermal expression below 4000 m. (c) Time series of the bottom water contributions to the SLR south of SAF (1000–4000 m) as marked by the magenta line in Figure 14b and below 4000 m. The blue bars represent *Purkey and Johnson*'s [2010] estimate with uncertainty ranges.

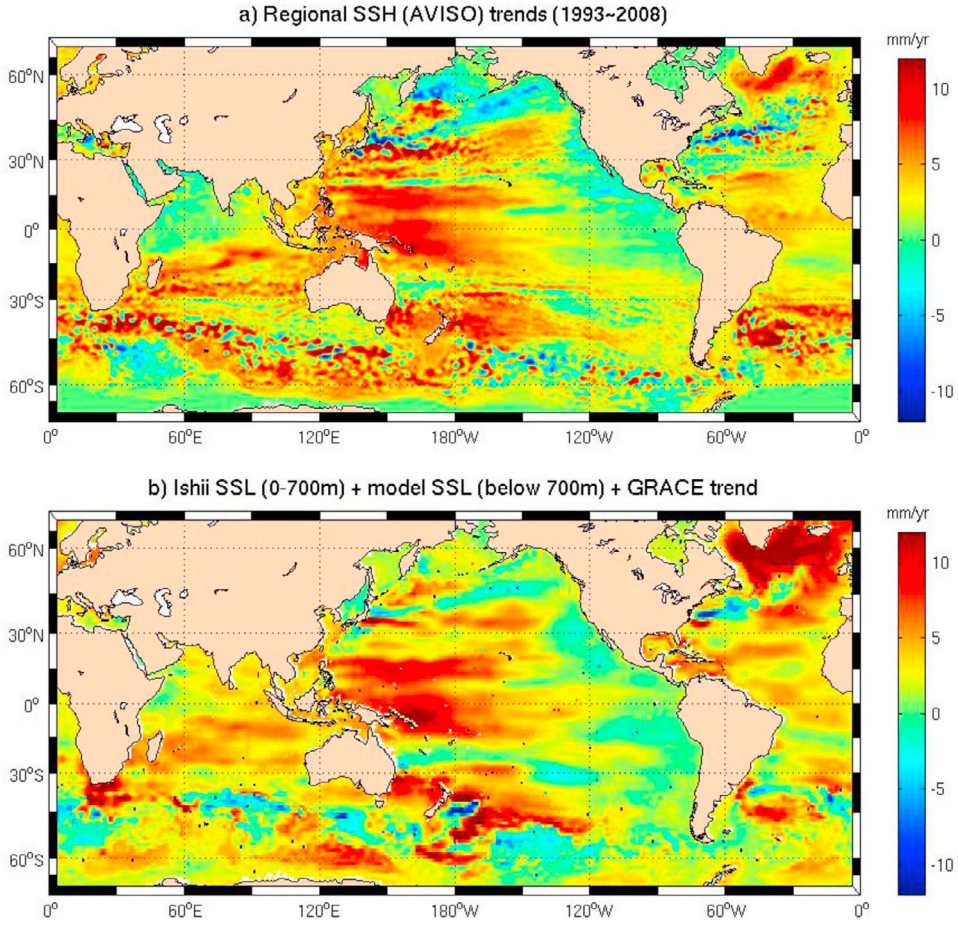

Figure 15. (a) Regional SSH trends derived from altimeters. (b) Combined trends from *Ishii and Kimoto* [2009] SSL data (0–700 m), model SSL (below 700 m), and a uniform GRACE trend of 0.85 mm/yr. The data-model combination explains most of the altimetry SLR. The overheated northern Atlantic subpolar gyre may be due to the lack of Greenland freshwater flux in the model.

go deeper, up to depth of 2000 m, but most abyssal oceans are still unmeasured. Therefore, ocean models are necessary to fill the data gaps.

5. Summary and Discussions

[36] In this paper, we have first assessed altimetry SSH, GRACE ocean bottom pressure, and in situ upper ocean steric sea level data with a focus on their seasonal variability and regional trends. The seasonal variability of altimetry data can be explained well by the upper ocean SSL, suggesting little contribution from deep oceans to the annual amplitude and phase maps of sea level changes. This makes sense because short-term surface heating and cooling stays or leaves the upper ocean layer in short timescales. This is also reproduced by our model.

[37] However, the story is different for the sea level trend maps. Our data assessment shows that the altimetry SLR cannot be explained by the sum of upper ocean (0–700 m) SSL and GRACE-derived ocean mass. This is true not only for their global means but also for their regional trends over the altimetry period. On global averages, they can only explain two-thirds of the observed sea level rise, leaving another one-third unexplained. One hypothesis that may explain the missing component of SLR is that the steric contribution from deep oceans below 700 m has not been accounted for in this budget.

[38] To test such a hypothesis, we have used a non-Boussinesq OGCM that is mass conserving instead of volume conserving and uses terrain-following coordinates instead of typical staircase approximations of the bathymetry. These model properties allow for a better representation of thermal expansion and deep water properties [*Huang and Jin*, 2002; *Gerdes*, 1993]. The model is calibrated and compared with a suite of data sets from satellite observations and in situ measurements in terms of their global means, basin averages, and regional trends for various periods of time. Particularly, the model is shown to be consistent with in situ upper ocean steric height [*Ishii and Kimoto*, 2009], upper ocean heat content [*Levitus et al.*, 2009], deep ocean temperature profiles [*Johnson et al.*, 2007, 2008a, 2008b], and bottom water measurements [*Purkey and Johnson*, 2010]. We have then used the model deep ocean SSL, combined it with the in situ upper ocean steric height, to create a full depth steric height. This combination is a proxy of the full depth ocean thermal expansion due to global

warming. Adding an extended ocean mass rate from *Domingues et al.* [2008] and GRACE data, it explains the altimetry sea level rise in both global means and regional trends.

[39] In summary, we have proposed a plausible hypothesis that deep ocean warming may have contributed up to one-third of the observed altimetry SLR. First, we emphasize the importance of maintaining heat and mass conservations and physical consistencies in ocean models (Figure 5). We understand that the model diagnosed deep ocean warming is not data, but the total heat added to the model is consistent with the estimate from the TOA radiation measurements, which is 0.9 ± 0.5 W m^{-2} for the entire Earth since 1985–2009 [*Trenberth and Carron*, 2001; *Trenberth and Fasullo*, 2010], roughly equivalent to the model heat flux of 1.05 W m^{-2}. On the other hand, heat content in the upper oceans (0–700 m) is known from various in situ observations [*Levitus et al.*, 2009] and the model apparently reproduces the upper ocean observations well (Figure 11). Therefore, the remaining heat has to be in the deep ocean. We have put a great effort to verify the model deep ocean warming, as shown in Figures 13–15. Such an approach to estimate deep ocean warming has not been done before. Second, we emphasize the important roles played by the oceanic circulation and dynamics in distributing heat within the global ocean and to the deep ocean. The innovative idea of this study is to explore the physical mechanisms of the ocean circulation and dynamics that distribute heat to the deep ocean in a unique pattern that explains the altimetry SLR not only in terms of its global mean, but also in its regional trends. Our results show that the deep ocean warming concentrates only in a few places where ocean circulation plays an important role (Figure 12). In addition, the deep ocean warming differs greatly from the upper ocean warming in geographical locations (compare Figure 3c with Figures 12c and 14a), indicating that the vertical diffusion is unlikely the cause. For example, *Masuda et al.* [2010] have shown that changes in the heat content of the deep ocean are far more sensitive to the air-sea thermal interchanges than previously considered. Clearly, more studies are needed for a better understanding of these oceanic processes that distribute heat in the deep ocean. Last, we emphasize the importance of continuous deep ocean observations not only for narrowing the gaps in the sea level budget, but also for improving ocean models, which are the primary tools for projecting future sea level changes and have played a key role in previous IPCC reports. This study seems to suggest that the deep ocean might have contributed to the present-day SLR more than previously thought [*Trenberth*, 2010]. If this is the case, the enormous heat stored in the deep ocean would have a profound effect on the climate and deserves a serious attention in projecting future sea level changes.

[40] **Acknowledgments.** This research is carried out at the Jet Propulsion Laboratory, California Institute of Technology, under contract with the National Aeronautics and Space Administration (NASA). Many thanks to C. Y. Kuo for providing his version of the upper ocean steric height data and S. G. Purkey and G. C. Johnson for the oceanic bottom water data. Discussions with V. Zlotnicki, J. Willis, and C. K. Shum are greatly appreciated.

References

Ablain, M., A. Cazenave, G. Valladeau, and S. Guinehut (2009), A new assessment of the error budget of global mean sea level rate estimated by satellite altimetry over 1993–2008, *Ocean Sci.*, *5*, 193–201, doi:10.5194/os-5-193-2009.

Bamber, J. L., R. B. Alley, and I. Joughim (2007), Rapid response of modern day ice sheets to external forcing, *Earth Planet. Sci. Lett.*, *257*, 1–13, doi:10.1016/j.epsl.2007.03.005.

Barnier, B., L. Siefridt, and P. Marchesiello (1995), Thermal forcing for a global ocean circulation model using a three-year climatology of ECMWF analyses, *J. Mar. Syst.*, *6*, 363–380, doi:10.1016/0924-7963(94)00034-9.

Budgell, W. P. (2005), Numerical simulation of ice-ocean variability in the Barents Sea region, *Ocean Dyn.*, doi:10.1007/s10236-005-0008-3.

Cazenave, A., K. Dominh, S. Guinehut, E. Berthier, W. Llovel, G. Ramillien, M. Ablain, and G. Larnicol (2009), Sea level budget over 2003–2008: A reevaluation from GRACE space gravimetry, satellite altimetry and Argo, *Global Planet. Change*, *65*, 83–88, doi:10.1016/j.gloplacha.2008.10.004.

Chambers, D. P. (2008), Converting release-04 gravity coefficients into maps of equivalent water thickness, report, 9 pp., Cent. for Space Res., Univ. of Texas at Austin, Austin, Texas.

Chen, J. L., C. R. Wilson, D. D. Blankenship, and B. D. Tapley (2009), Accelerated Antarctic ice loss from satellite gravity measurements, *Nat. Geosci.*, *2*, 859–862, doi:10.1038/NGEO694.

Cheng, X., and Y. Qi (2007), Trends of sea level variations in the South China Sea from merged altimetry data, *Global Planet. Change*, *57*, 371–382, doi:10.1016/j.gloplacha.2007.01.005.

Church, J. A., P. L. Woodworth, T. Aarup, and W. S. Wilson (Eds.) (2010), *Understanding Sea-Level Rise and Variability*, Wiley-Blackwell, Hoboken, N. J.

Conkright, M. E., R. A. Locarnini, H. E. Garcia, T. D. O'Brien, T. P. Boyer, C. Stephens, and J. I. Antonov (2002), World ocean atlas 2001: Objective analyses, data statistics, and figures [CD-ROM], *Intern. Rep. 17*, Natl. Oceanogr. Data Cent., Silver Spring, Md.

Domingues, C. M., J. A. Church, N. J. White, P. J. Glecker, S. E. Wijffels, P. M. Barker, and J. R. Dunn (2008), Improved estimates of upper-ocean warming and multi-decadal sea-level rise, *Nature*, *453*, 1090–1093, doi:10.1038/nature07080.

Duan, X. J., J. Y. Guo, C. K. Shum, and W. van der Wal (2009), On the post-processing removal of correlated errors in GRACE temporal gravity field solutions, *J. Geod.*, *83*, 1095–1106, doi:10.1007/s00190-009-0327-0.

Gerdes, R. (1993), A primitive equation ocean circulation model using a general vertical coordinate transformation: 1. Description and testing the model, *J. Geophys. Res.*, *98*, 14,683–14,701, doi:10.1029/93JC00760.

Greatbatch, R. J. (1994), A note on the represent of steric sea level in models that conserve volume rather than mass, *J. Geophys. Res.*, *99*, 12,767–12,771, doi:10.1029/94JC00847.

Greatbatch, R. J., and Y. Lu (2001), Relaxing the Boussinesq approximation in ocean circulation models, *J. Atmos. Oceanic Technol.*, *18*, 1911–1923, doi:10.1175/1520-0426(2001)018<1911:RTBAIO>2.0.CO;2.

Gregory, J. M., H. T. Banks, P. A. Stott, J. A. Lowe, and M. D. Palmer (2004), Simulated and observed decadal variability in ocean heat content, *Geophys. Res. Lett.*, *31*, L15312, doi:10.1029/2004GL020258.

Guo, J. Y., X. J. Duan, and C. K. Shum (2010), Non-isotropic filtering and leakage reduction for determining mass changes over land and ocean using GRACE data, *Geophys. J. Int.*, *181*, 290–302, doi:10.1111/j.1365-246X.2010.04534.x.

Haidvogel, D. B., and A. Beckmann (1999), *Numerical Ocean Circulation Modeling*, 318 pp., Imperial Coll. Press, London.

Han, S.-C., C. K. Shum, M. Bevis, C. Ji, and C.-Y. Kuo (2006), Crustal dilatation observed by GRACE after the 2004 Sumatra-Andaman earthquake, *Science*, *313*, 658–662, doi:10.1126/science.1128661.

Huang, R. X., and X. Jin (2002), Sea surface elevation and bottom pressure anomalies due to thermohaline forcing, part I: Isolated perturbations, *J. Phys. Oceanogr.*, *32*, 2131–2150, doi:10.1175/1520-0485(2002)032<2131:SSEABP>2.0.CO;2.

Ishii, M., and M. Kimoto (2009), Reevaluation of historical ocean heat content variations with time-varying XBT and MBT depth bias corrections, *J. Oceanogr.*, *65*, 287–299, doi:10.1007/s10872-009-0027-7.

Johnson, G. C., and S. C. Doney (2006), Recent western South Atlantic bottom water warming, *Geophys. Res. Lett.*, *33*, L14614, doi:10.1029/2006GL026769.

Johnson, G. C., B. Mecking, B. M. Sloyan, and S. E. Wijffels (2007), Recent bottom water warming in the Pacific Ocean, *J. Clim.*, *20*, 5365–5375, doi:10.1175/2007JCI1879.1.

Johnson, G. C., S. G. Purkey, and J. L. Bullister (2008a), Warming and freshening in the abyssal southeast Indian Ocean, *J. Clim.*, *21*, 5351–5363, doi:10.1175/2008JCLI2384.1.

Johnson, G. C., S. G. Purkey, and J. M. Toole (2008b), Reduced Antarctic meridional ocerturning circulation reaches the North Atlantic Ocean, *Geophys. Res. Lett.*, *35*, L22601, doi:10.1029/2008GL035619.

Kalnay, E., et al. (1996), The NCEP/NCAR, 40-year reanalysis project, *Bull. Am. Meteorol. Soc.*, *77*, 437–471, doi:10.1175/1520-0477(1996)077<0437:TNYRP>2.0.CO;2.

Kuo, C., C. Shum, A. Braun, K. Cheng, and Y. Yi (2008), Vertical motion determined using satellite altimetry and tide gauges, *Terr. Atmos. Oceanic Sci.*, *19*, 21–35, doi:10.3319/TAO.2008.19.1-2.21(SA).

Leuliette, E. W., and L. Miller (2009), Closing the sea level rise budget with altimetry, Argo, and GRACE, *Geophys. Res. Lett.*, *36*, L04608, doi:10.1029/2008GL036010.

Levitus, S., J. I. Antonov, T. P. Boyer, R. A. Locarnini, H. E. Garcia, and A. V. Mishonov (2009), Global ocean heat content 1955–2008 in light of recently revealed instrumentation problems, *Geophys. Res. Lett.*, *36*, L07608, doi:10.1029/2008GL037155.

Lombard, A., D. Garcia, G. Ramillien, A. Cazenave, R. Biancale, J. Lemoine, F. Flechtner, R. Schmidt, and M. Ishii (2007), Estimation of steric sea level variations from combined GREACE and Jason-1 data, *Earth Planet. Sci. Lett.*, *254*, 194–202, doi:10.1016/j.epsl.2006.11.035.

Losch, M., A. Adcroft, and J. Campin (2004), How sensitive are coarse general circulation models to fundamental approximations in the equations of motion?, *J. Phys. Oceanogr.*, *34*, 306–319, doi:10.1175/1520-0485(2004)034<0306:HSACGC>2.0.CO;2.

Masuda, S., et al. (2010), Simulated rapid warming of abyssal north Pacific waters, *Science*, *329*, 319–322, doi:10.1126/science.1188703.

Meredith, M. P., A. C. Garabato, A. L. Gordon, and G. C. Johson (2008), Evolution of the deep and bottom waters of the Scotia Sea, Southern Ocean, during 1995–2005, *J. Clim.*, *21*, 2237–3343, doi:10.1175/2007JCLI2238.1.

Milne, G. A., W. R. Gehrels, C. W. Hughes, and M. A. Tamisiea (2009), Identifying the causes of sea-level change, *Nat. Geosci.*, *2*, 471–478, doi:10.1038/ngeo544.

Paulson, A., S. Zhong, and J. Wahr (2007), Inference of mantle viscosity from GRACE and relative sea level data, *Geophys. J. Int.*, *171*, 497–508, doi:10.1111/j.1365-246X.2007.03556.x.

Peltier, R. (2009), Closure of the budget of global sea level rise over the GRACE era: The importance and magnitudes of the required corrections for global glacial isostatic adjustment, *Quat. Sci. Rev.*, *28*, 1658–1674, doi:10.1016/j.quascirev.2009.04.004.

Peltier, W. (2004), Global glacial isostasy and the surface of the ice-age Earth: The ICE-5G (VM2) model and GRACE, *Annu. Rev. Earth Planet. Sci.*, *32*, 111–149, doi:10.1146/annurev.earth.32.082503.144359.

Ponte, R. (1999), A preliminary model study of the large-scale seasonal cycle in bottom pressure over the global ocean, *J. Geophys. Res.*, *104*, 1289–1300, doi:10.1029/1998JC900028.

Purkey, S. G., and G. C. Johnson (2010), Warming of global abyssal and deep southern ocean waters between the 1990s and 2000s: Contributions to global heat and sea level rise, *J. Clim.*, *23*, 6336–6351, doi:10.1175/2010JCLI3682.1.

Rignot, E., J. L. Bamber, M. R. van den Broeke, C. Davis, Y. Li, W. J. van de Berg, and E. van Meijgaard (2008), Recent Antarctic ice mass loss from radar interferometry and regional climate modeling, *Nat. Geoci.*, *1*, 106–110, doi:10.1039/ngeo102.

Shchepetkin, A., and J. C. McWilliams (2005), The regional oceanic modeling system (ROMS): A split-explicit, free-surface, topography-following-coordinate oceanic model, *Ocean Modell.*, *9*, 347–404, doi:10.1016/j.ocemod.2004.08.002.

Song, Y., and D. Haidvogel (1994), A semi-implicit primitive equation ocean circulation model using a generalized topography-following coordinate system, *J. Comput. Phys.*, *115*, 228–244, doi:10.1006/jcph.1994.1189.

Song, Y. T., and S. C. Han (2011), Satellite observations defying the long-held tsunami genesis theory, in *Remote Sensing of Global Ocean Changes*, doi:10.1007/978-3-642-16541-2, Springer, Berlin, in press.

Song, Y. T., and T. Y. Hou (2006), Parametric vertical coordinate formulation for multiscale, Boussinesq, and non-Boussinesq ocean modeling, *Ocean Modell.*, *11*, 298–332, doi:10.1016/j.ocemod.2005.01.001.

Song, Y. T., and V. Zlotnicki (2008), Subpolar ocean bottom pressure oscillation and its links to the tropical ENSO, *Int. J. Remote Sens.*, *29*, 6091–6107, doi:10.1080/01431160802175538.

Song, Y. T., R. Gross, X. Wang, and V. Zlotnicki (2011), A non-Boussinesq terrain-following OGCM for oceanographic and geodetic applications, *Adv. Geosci.*, *18*, 63–86.

Stroeve, J., and W. Meier (1999), Sea Ice Trends and Climatologies from SMMR and SSM/I, June–December 2007, http://nsidc.org/data/smmr_ssmi_ancillary/area_extent.html, Natl. Snow and Ice Data Cent., Boulder, Colo. (Updated 2008.)

Swenson, S., and J. Wahr (2006), Post-processing removal of correlated errors in GRACE data, *Geophys. Res. Lett.*, *33*, L08402, doi:10.1029/2005GL025285.

Swenson, S., D. Chambers, and J. Wahr (2008), Estimating geocenter variations from a combination of GRACE and ocean model output, *J. Geophys. Res.*, *113*, B08410, doi:10.1029/2007JB005338.

Tapley, B. D., S. Bettadpur, J. Ries, P. Thompson, and M. Watkins (2004), GRACE measurements of mass variability in the Earth system, *Science*, *305*, 503–505, doi:10.1126/science.1099192.

Trenberth, K. E. (2010), The ocean is warming, isn't it?, *Nature*, *465*, 304, doi:10.1038/465304a.

Trenberth, K. E., and J. M. Carron (2001), Estimates of meridional atmosphere and ocean heat transports, *J. Clim.*, *14*, 3433–3443, doi:10.1175/1520-0442(2001)014<3433:EOMAAO>2.0.CO;2.

Trenberth, K. E., and J. T. Fasullo (2010), Tracking earth's energy, *Science*, *328*, 316–317, doi:10.1126/science.1187272.

Velicogna, I. (2009), Increasing rates of ice mass loss from the Greenland and Antarctic ice sheets revealed by GRACE, *Geophys. Res. Lett.*, *36*, L19503, doi:10.1029/2009GL040222.

Willis, J. K., D. Roemmick, and B. Cornelle (2004), Interannual variability in upper ocean heat content, temperature, and thermosteric expansion on global scales, *J. Geophys. Res.*, *109*, C12036, doi:10.1029/2003JC002260.

Willis, J. K., D. P. Chambers, and R. S. Nerem (2008), Assessing the globally averaged sea level budget on seasonal to interannual timescales, *J. Geophys. Res.*, *113*, C06015, doi:10.1029/2007JC004517.

Willis, J. K., J. M. Lyman, G. C. Johnson, and J. Gilson (2009), In situ data biases and recent ocean heat content variability, *J. Atmos. Oceanic Technol.*, *26*, 846–852, doi:10.1175/2008JTECHO608.1.

Wu, X., M. B. Heflin, H. Schotman, B. L. A. Vermeersen, D. Dong, R. S. Gross, E. R. Ivins, A. W. Moore, and S. E. Owen (2010), Simultaneous estimation of global present-day water transport and glacial isostatic adjustment, *Nat. Geosci.*, *3*, 642–646, doi:10.1038ngo938.

Wunsch, C., R. M. Ponte, and P. Heimbach (2007), Decadal trends in sea level patterns: 1993–2004, *J. Clim.*, *20*, 5889–5911, doi:10.1175/2007JCLI1840.1.

Yin, J., M. E. Schlesinger, and R. J. Stouffer, (2009), Model projections of rapid sea-level rise on the northeast coast of the United States, *Nat. Geosci.*, *2*, 262–266, doi:10.1038/NGEO468.

Zlotnicki, V., J. Wahr, I. Fukumori, and Y. T. Song (2007), The antarctic circumpolar current: Transport variability during 2002–2005, *J. Phys. Oceanogr.*, *37*, 230–244, doi:10.1175/JPO3009.1.

F. Colberg, CSIRO Marine and Atmospheric Research, 107-121 Station St., Aspendale, Vic 3195, Australia.

Y. T. Song, Jet Propulsion Laboratory, California Institute of Technology, 4800 Oak Grove Drive, Pasadena, CA 91109, USA. (yuhe.t.song@jpl.nasa.gov)